ChemMedChem

Research Article
doi.org/10.1002/cmdc.202400057

Chemistry Europe
European Chemical Societies Publishing

www.chemmedchem.org

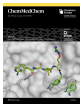

Fragment-Based Design, Synthesis, and Characterization of Aminoisoindole-Derived Furin Inhibitors

Roman W. Lange,[a] Konstantin Bloch,[b] Miriam Ruth Heindl,[b] Jan Wollenhaupt,[c] Manfred S. Weiss,[c] Hans Brandstetter,[d] Gerhard Klebe,[a] Franco H. Falcone,[e] Eva Böttcher-Friebertshäuser,[b] Sven O. Dahms,*[a, d] and Torsten Steinmetzer*[a]

A 1*H*-isoindol-3-amine was identified as suitable P1 group for the proprotein convertase furin using a crystallographic screening with a set of 20 fragments known to occupy the S1 pocket of trypsin-like serine proteases. Its binding mode is very similar to that observed for the P1 group of benzamidine-derived peptidic furin inhibitors suggesting an aminomethyl substitution of this fragment to obtain a couplable P1 residue for the synthesis of substrate-analogue furin inhibitors. The obtained inhibitors possess a slightly improved picomolar inhibitory potency compared to their benzamidine-derived analogues. The crystal structures of two inhibitors in complex with furin revealed that the new P1 group is perfectly suited for incorporation in peptidic furin inhibitors. Selected inhibitors were tested for antiviral activity against respiratory syncytial virus (RSV) and a furin-dependent influenza A virus (SC35M/H7N7) in A549 human lung cells and demonstrated an efficient inhibition of virus activation and replication at low micromolar or even submicromolar concentrations. First results suggest that the Mas-related G-protein coupled receptor GPCR-X2 could be a potential off-target for certain benzamidine-derived furin inhibitors.

Introduction

The type-1 membrane-bound serine endoprotease furin belongs to the family of human proprotein convertases (PCs) and contains a Ca^{2+}-dependent subtilisin-like protease domain. Together with six additional members of the PC family such as PC1, PC2, PC4, PACE4, PC5/6, and PC7, it activates numerous human proproteins C-terminal of a multibasic R/K-X_n-R/K↓ recognition sequence, where X_n is a 0, 2, 4, or a 6-amino acid spacer.[1,2] These basic PCs have been implicated in numerous diseases including cancer, atherosclerosis, cystic fibrosis, rheumatoid arthritis, obesity, and neurodegenerative disorders,[3–7] which has stimulated the development of various types of synthetic PC inhibitors.[8] Furin-like PCs have also emerged as potential targets for the treatment of infectious diseases, because they activate numerous surface glycoproteins[9] of pathogenic viruses and bacterial toxins. During the coronavirus disease 2019 (COVID-19) pandemic, furin gained a lot of attention as an essential host protease for the replication of severe acute respiratory syndrome coronavirus 2 (SARS-CoV-2). Compared to SARS-CoV that caused an outbreak of severe respiratory infections in 2002/2003, a four amino acid insertion provided a minimal R-R-A-R685↓ furin cleavage site at the S1/S2 site in the spike (S) protein of SARS-CoV-2. The ubiquitous distribution of furin leads to a more efficient S protein activation and enhanced virus replication in all infected tissues. Furthermore, the acquired furin dependency facilitates the transmissibility of SARS-CoV-2 leading to the pandemic. Consequently, furin inhibitors showed antiviral activities against several furin-dependent viruses including SARS-CoV-2.[10,11]

Incorporation of the arginine mimetic 4-aminomethylbenzamidine (Amba) at the P1 position improved the potency of substrate-like furin inhibitors to low picomolar K_i values.[12,13] A reduction of the net charge of such inhibitors by substitution of highly basic arginine by less basic canavanine residues at the P2- and P4-positions resulted in an increased antiviral potency of the inhibitors in cell culture. More importantly, the incorporation of canavanine provided inhibitors with significantly reduced toxicity compared to their arginine analogues.[14] Thus, we were interested in identifying less basic replacements of the Amba residue also at the P1 position, which maintain furin affinity and might further reduce the toxicity of the inhibitors. An overview of our previously developed Amba-derived furin inhibitors is provided as Figure S1 in the supporting information.

[a] *R. W. Lange, G. Klebe, S. O. Dahms, T. Steinmetzer*
Institute of Pharmaceutical Chemistry, Philipps University, Marbacher Weg 6–10, D-35032 Marburg, Germany
Phone: +49 6421 2825900
E-mail: sven.dahms@plus.ac.at
steinmetzer@uni-marburg.de

[b] *K. Bloch, M. R. Heindl, E. Böttcher-Friebertshäuser*
Institute of Virology, Philipps University, Hans-Meerwein-Str. 2, Marburg, Germany

[c] *J. Wollenhaupt, M. S. Weiss*
Macromolecular Crystallography, Helmholtz-Zentrum Berlin, 12489 Berlin, Germany

[d] *H. Brandstetter, S. O. Dahms*
Department of Biosciences, University of Salzburg, Billrothstrasse 11, A-5020 Salzburg, Austria
Phone: +43 662 8044 7277

[e] *F. H. Falcone*
Institute of Parasitology, BFS, Justus Liebig University, 35392 Giessen, Germany

Meanwhile, we could establish a reliable protocol for the crystallization of ligand-free furin suitable for soaking of peptidic and small molecule inhibitors.[14–19] Using an optimized soaking procedure, furin crystals might also be suitable for crystallographic screening of low affinity fragments with typical K_d-values in a range of 0.1–10 mM.[20] Among 20 selected fragments, we identified a 1*H*-isoindol-3-amine as potential P1 residue. This fragment was converted into an aminomethyl-substituted derivative suitable for incorporation into substrate-analogue inhibitors. In this paper we describe the enzyme kinetic characterization of these inhibitors and their structure determination in complex with furin. Furthermore, the antiviral potency of the inhibitors against a mouse-adapted highly pathogenic avian influenza A virus (SC35M) and respiratory syncytial virus (RSV) was demonstrated in cell-based assays.

Results

Screening of Arginine-Like Fragments to Identify New P1 Binders of Furin

Substitutions of the Amba residue at the P1 position by less basic groups always strongly reduced the potency of substrate-analogue inhibitors in previous studies.[21] To overcome this challenge, we applied a crystallographic fragment screening approach with a selection of compounds that a) previously bound to the S1 substrate binding pockets of trypsin-like serine proteases or b) might serve as P1 arginine mimetics for furin inhibitors with a lower pK_a than benzamidine. For soaking of fragments, we used an optimized condition of ligand-free furin crystals with reduced NaCl-concentration (1 M instead of 3.3 M NaCl) and 20% DMSO. This condition allows the binding of low and medium affinity ligands and improves the solubility of hydrophobic compounds. As control compound we soaked benzamidine (**F1**), which inhibits furin with a K_i value of 0.75 mM[22] in a typical affinity range for fragments, usually 0.1–10 mM.[20] Indeed, fragment **F1** showed high occupancy (89%) at the S1 pocket of furin at a concentration of 200 mM (labeled as 1_{S1} in Figure S4A). A second binding site of **F1** was observed at a crystal contact (Figure S4B, labeled as 1_{CC}) with 76% occupancy. This result shows that even weak binding fragments can be soaked into the substrate binding pocket of furin and thus prove the feasibility of our screening approach.

Soaking of the fragments was performed at 100 mM overnight. If damage of the crystals was observed during soaking, the compound concentration was reduced to 20 mM. Before hit identification, all measured datasets were subjected to a refinement pipeline, largely improving the hit rate in previous screening campaigns.[23] Hits were identified by manual inspection of the $2\mathbf{F}_o$-$\mathbf{F}_c$ and $\mathbf{F}_o$-$\mathbf{F}_c$ electron density maps as well as by evaluation of event maps calculated with PanDDA.[24] Out of the 20 investigated compounds (Figure S5), we identified 2 additional S1-pocket binders, 1*H*-isoindol-3-amine **F2** (Table S2, labeled as 2_{S1} in Figure S6A and thiophene-3-carboximidamid, **F3**, Figure S6B). We also observed binding of compound **F2** at the S4-pocket of furin with a lower occupancy of 64% compared to 100% at the S1-pocket, indicating a weaker affinity at this position (Figure S6C, labeled as 2_{S4}). Binding of fragment **F2** was also observed at crystal contacts, which are not relevant for inhibitor development (Figure S6C, labeled as 2_{CC}). Binding at this crystal contact was also observed for other flat compounds that are able to stack between Arg268 of two symmetry related furin molecules.[15]

In this study we focused on fragment **F2**, showing a significantly reduced pK_a-value compared to benzamidine (pK_a = 11.6, Figure 1).

Fragment **F2** adopted an almost identical binding pose compared to benzamidine (**F1**) and the 4-aminomethyl-benzamidine P1 residue of a typical substrate-like inhibitor (e.g., compound **4**, also named as **MI-1148** and initially described as #19 in our previous publication,[12] Figure 2). Interestingly, the amidino group of benzamidine (**F1**) was found in hydrogen bonding distance to Asp258 (Figure 2A) which was not observed for the P1 residue of inhibitor **MI-1148** and fragment **F2** (Figure 2B). Notably, we did not observe a complete transition of furin from the OFF- to the ON-state upon binding of fragments **F1** and **F2**. This is indicated by octahedral coordination of the sodium binding site with six polar contacts (Figure 2). Binding of substrate-like inhibitors usually induce a tetragonal-pyramidal coordination of the sodium ion with only five interactions caused by a break of the hydrogen bond between the side chain hydroxyl groups of Ser316 and Thr309.[16]

Synthesis of Precursors

To incorporate fragment **F2** as P1 residue in substrate-like peptidic inhibitors, we developed a synthesis strategy for an aminomethyl-derivative. The synthesis of the required 6-(aminomethyl)-1*H*-isoindole-3-amine (Amia) started from 2,4-dimethylbenzonitrile **5** (Scheme 1). Its bromination provided the corresponding 2,4-bis(bromomethyl)benzonitrile **6**, which was converted to intermediate **7** by Gabriel synthesis. The final removal of the phthaloyl protection groups using methylamine resulted in a simultaneous cyclization and provided the Amia group **8**. A negligible product formation was observed in initial attempts when using hydrazine for phthaloyl removal.

The protected precursor of the P5 group **13** required for the synthesis of inhibitor **18** was prepared as shown in Scheme 2. 2-(4-iodophenyl)acetic acid **9** was coupled with benzyl allylcarba-

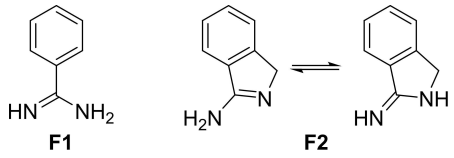

Figure 1. Structures of ligands **F1** and **F2**. Semi-empirical MNDO (Modified Neglect of Diatomic Overlap) calculations performed in a previous study[25] revealed that fragment **F2** exist with similar amounts in its tautomeric 1*H*-isoindol-3-amine (left structure, 45%) and isoindolin-1-imine (right, 55%) forms, possessing calculated pK_a values of approximately 9.4 and 10.4 (calculated with MarvinSketch 17.17.0, ChemAxon Ltd.), respectively.

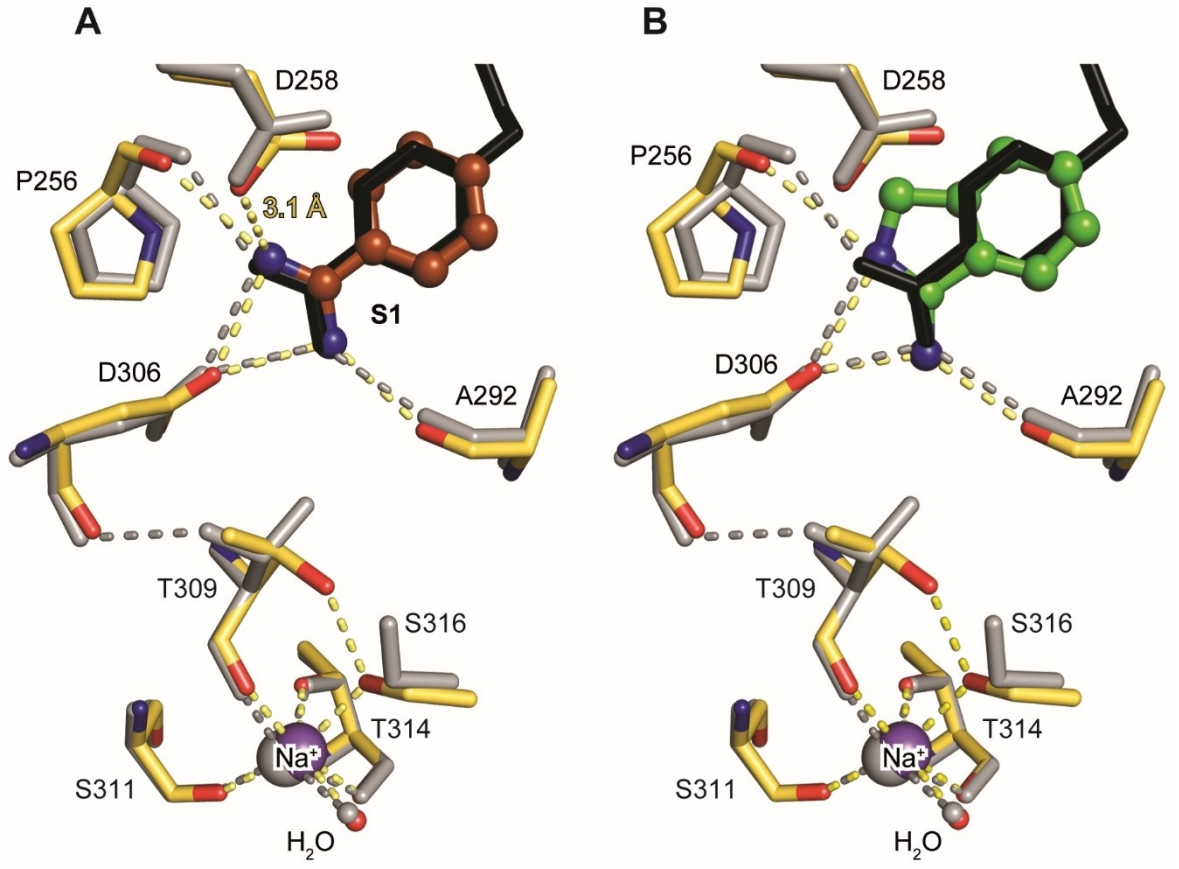

Figure 2. Interactions of fragments **F1** and **F2** in the S1 pocket of furin. Superposition of furin bound to (A) fragment **F1** (brown) and (B) compound **F2** (green) with furin (yellow carbons) in complex with the substrate-like inhibitor **MI-1148** (4-guanidinomethyl-phenylacetyl-Arg-Tle-Arg-4-aminomethyl-benzamidine in black (structure given in Figure S1), furin in grey, PDB-ID: 4RYD[12]). Important interactions of **F1** and **F2** with furin (yellow) or of the substrate-like inhibitor with furin (grey) are highlighted as dashed lines.

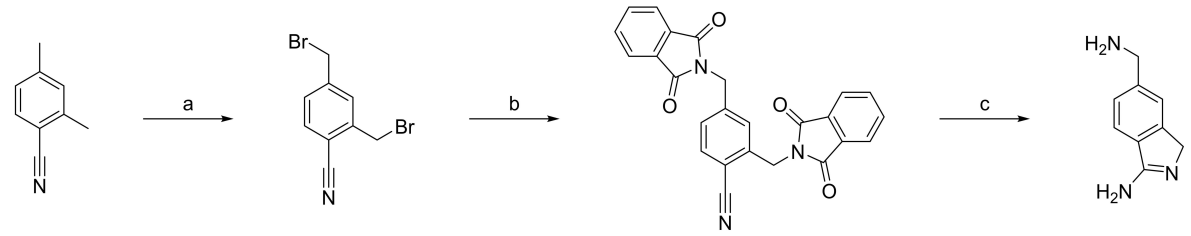

5 **6** **7** **8**

Scheme 1. Synthesis of 6-(aminomethyl)-1*H*-isoindole-3-amine **8**. a) NBS, AIBN in ACN 140 °C in a microwave, 4 h; b) potassium phthalimide in DMF, 100 °C, 1 h; c) $MeNH_2$ in EtOH, reflux, 3 h, and purification by preparative HPLC.

mate **10** under Heck-conditions and provided intermediate **11**, which was subsequently hydrogenated with Pd/C as catalyst under ambient pressure. Due to incomplete removal of the Cbz protection, the intermediate was additionally treated with 4 M HBr in AcOH and provided compound **12**. Treatment with Boc_2O resulted in the P5 building block **13**, which could be used in solid phase peptide synthesis (SPPS).

Synthesis of Inhibitors

The inhibitors were synthesized by an identical strategy as previously described.[14,21] Briefly, the P5-P2 segments of the inhibitors were prepared by standard Fmoc solid phase peptide synthesis on 2-chlorotrityl chloride resin. The cleavage of the peptides from the resin under mild acidic conditions provided the fully side chain protected P5-P2 segments, e.g., intermediate **14**, which was coupled with the Amia residue **8**. The removal of all protecting groups in the final step yielded inhibitor **17** (Scheme 3). The related inhibitors **15**, **16**, and **18**

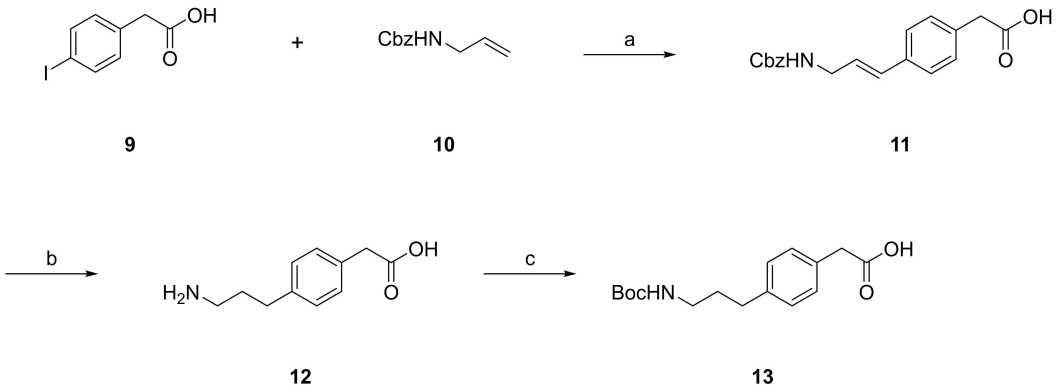

Scheme 2. Synthesis of compound **13**. a) $Pd(OAc)_2$, K_2CO_3 in DMF, 140 °C, 30 min; b) i) H_2, Pd/C in EtOH, r.t., 40 h; ii) 33 % HBr/AcOH, r.t., 2 h; c) 0.5 M NaOH, Boc_2O in 1,4-dioxane, r.t., overnight.

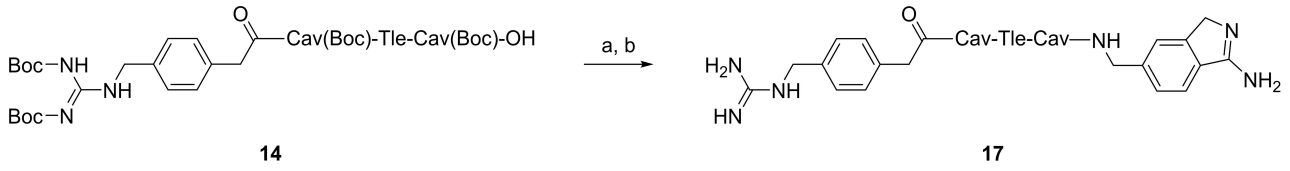

Scheme 3. Synthesis of inhibitor **17**. Intermediate **14** was prepared on 2-chlorotrityl chloride resin as described previously.[14] a) 1.0 equiv. of 6-(aminomethyl)-1*H*-isoindole-3-amine·2 TFA, 1.65 eq PyBOP, and 4 equiv. of DIPEA and 4.5 eq 6-Cl-HOBt in DMF; (b) TFA/TIS/H_2O (95 : 2.5 : 2.5 v/v/v), 7.5 h at r.t., precipitation in diethyl ether, followed by preparative RP-HPLC.

were prepared by the same strategy using different P2 and P4 residues or P5 groups. Their structures are summarized in Table 1.

Enzyme Kinetic Measurements

All enzyme kinetic measurements were performed with the optimized substrate Ac–Arg–Arg–Tle–Arg–Arg–AMC[26] at a final furin concentration of approximately 95 pM in the assay. The use of this low furin concentration allows calculation of K_i values for very potent inhibitors with equation 1 (see experimental section) for classical reversible competitive inhibitors.

Table 1. Structures and potencies of the synthesized furin inhibitors.

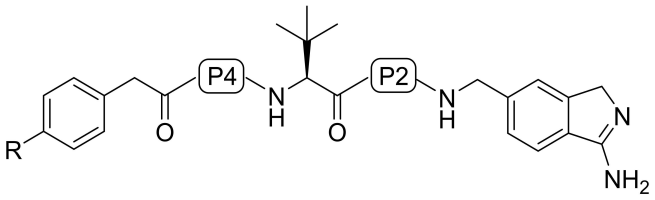

No.	R	P4	P2	K_i (pM)	k_{on} ($M^{-1}s^{-1}$)	k_{off} (s^{-1})
15	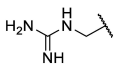	Arg	Lys	4.78 ± 0.19	1.72×10^{8}	8.22×10^{-4}
16		Cav[a]	Cav	22.1 ± 0.8	1.02×10^{7}	2.25×10^{-4}
17	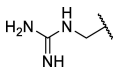	Cav	Cav	7.08 ± 0.44	1.33×10^{8}	9.42×10^{-4}
18	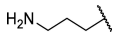	Cav	Cav	44.2 ± 1.1	2.82×10^{7}	1.24×10^{-3}

[a]Cav: 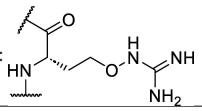

This avoids tight-binding conditions, where the exact active enzyme concentration is required for K_i calculations. At these conditions, biphasic progress curves containing an initial non-linear part followed by a linear steady-state segment were observed for all inhibitors (Figure 3A). This behavior is characteristic for a slow-binding inhibition, which in addition to the K_i value determination also allows the calculation of the association and dissociation rate constants k_{on} and k_{off}, respectively. The progress curves were fitted to equation 2, providing the final steady-state velocities v_s and a first-order rate constant k_{obs} for the initial nonlinear part. The v_s values as function of the inhibitor concentrations were used for K_i value calculation with equation 1 (Figure 3B). The association rate constants k_{on} were obtained by fitting the k_{obs} values against the inhibitor concentration with equation 3 (Figure 3C). The k_{off} values were calculated from the known K_i and k_{on} values using equation 4. The determined kinetic constants of all inhibitors are summarized in Table 1.

The first inhibitor **15** of this series containing the Amia residue inhibits furin with a K_i value of 4.78 pM, which is nearly twofold stronger as described for the analogous P1 Amba inhibitor ($K_i = 8.5$ pM, inhibitor #27 in our previous publication[21]). In the other inhibitors we have incorporated canavanine in P2 and P4 positions, which is a structurally related less basic analog of arginine. Due to its oxyguanidine, it possesses a significantly reduced side chain pK_a value of 7.01.[27] In previous work we could demonstrate that the replacement of arginine by canavanine provides peptidic furin inhibitors with reduced toxicity compared to their Arg analogues.[14] Slightly enhanced potencies of 22.1 pM and 7.08 pM were found for inhibitors **16** and **17**, respectively, when compared with their Amba analogues ($K_i = 34.2$ pM and 10.1 pM for inhibitors #7 and #8 in our previous publication[14]).

From previous studies we knew that inhibitors with an aminomethyl substitution in para position of the P5 phenylacetyl group revealed a reduced toxicity compared with their guanidinomethyl-substituted analogs, probably to their slightly reduced basicity.[14] However, these aminomethyl derivatives showed a reduced inhibitory potency against furin in enzyme kinetic studies, which could be explained by a different binding mode in the S5 pocket. The aminomethyl group is only involved in a single interaction with the side chain of Asp264 in the so-called $S5_2$ subsite. In contrast, the elongated guanidinomethyl group is directed toward the $S5_1$ subsite and involved in a complex H-bond network to Asp236, Val231 and via a water molecule to Asp233, Ala267 and Asp236.[18,28] We speculated that the increased length of the P5 substituent of inhibitor **18** enables improved S5 interactions by addressing the $S5_1$ subsite. However, a nearly 2-fold reduced inhibitory potency was found for the elongated inhibitor **18** compared with analog **16**.

Structure of Amia-Derived Inhibitors Bound to Furin

The binding mode of two Amia-derived inhibitors **15** and **17** in complex with furin was determined by X-ray crystallography. The inhibitors were well defined in the electron density map (Figure S7). However, the electron density map at the guanidinomethyl-group of compound **17** (Figure S7B) was less well defined compared to the equivalent site of inhibitor **15** (Figure S7A). Interestingly, we observed a similar behavior for other inhibitors with canavanine at P4 position in previous studies.[14] The overall binding poses of compounds **15** (Figure 4A) and **17** (Figure 4B) is very similar to the prototypic substrate-like inhibitor **MI-1148**.[12] Thus, displacement of Amba by Amia did not interfere with any enzyme-inhibitor-interactions. This observation is in excellent agreement with the similar K_i-values measured for the Amba and Amia derivates, which were both in the low pM range (Table 1).

Toxicity Study with Inhibitor 17

In two previous publications we had reported the results from toxicity studies with several Amba-derived peptidic furin inhibitors in mice.[14,21] Based on the tested compounds so far, the highest toxicity was found for inhibitor **MI-1148**, whereas the lowest toxicity was found for its P2 and P4 canavanine

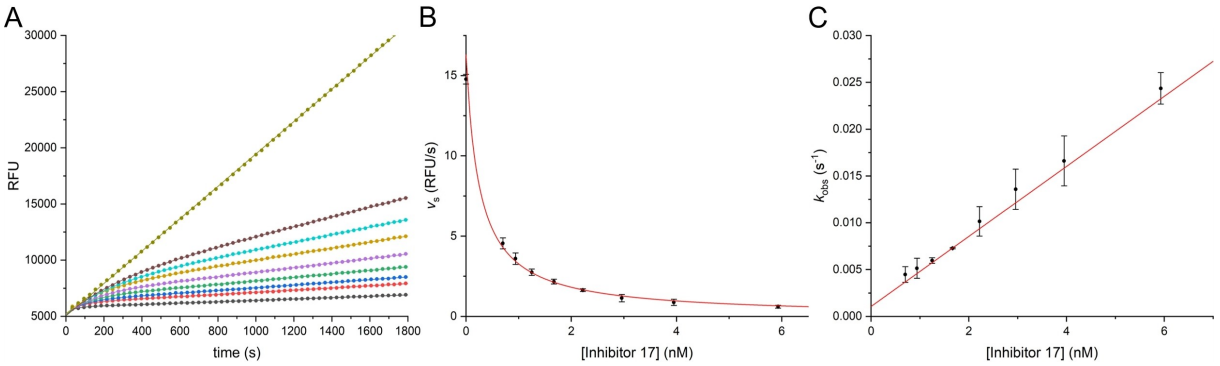

Figure 3. Inhibition of furin (0.095 nM) by inhibitor **17** in presence of substrate Ac–Arg–Arg–Tle–Arg–Arg–AMC (50 μM). (A) The progress curves at inhibitor concentrations of 5.93 nM (black), 3.95 nM (red), 2.96 nM (blue), 2.22 nM (green), 1.67 nM (purple), 1.25 nM (gold), 0.94 nM (cyan) and 0.70 nM (brown) were fitted to equation 2. The linear control measurement in absence of inhibitor is given in yellow-green. (B) Calculation of the K_i value by fitting the v_s values as functions of the inhibitor concentrations with equation 1. (C) Fitting of the k_{obs} values as function of the inhibitor concentrations with equation 3 provided the k_{on} value. The determined K_i and k_{on} values were used for the calculation of k_{off} with equation 4.

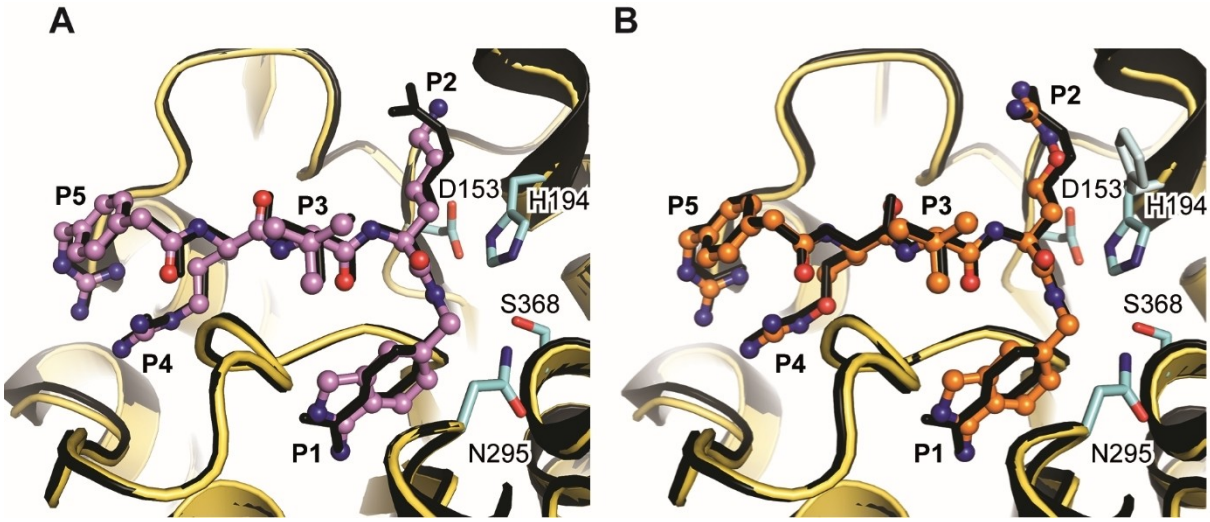

Figure 4. X-ray structures of furin in complex with Amia-derived inhibitors **15** and **17**. Furin and the inhibitors are shown as cartoon (yellow) and ball-and-stick model, respectively. Structures of furin in complex with (A) inhibitor **15** (violet) and (B) inhibitor **17** (orange) are superimposed with furin bound to the Amba-based inhibitor **MI-1148** (4-guanidinomethyl-phenylacetyl-Arg-Tle-Arg-Amba in black).

analogue **MI-1851** (4-guanidino-phenylacetyl-Cav-Tle-Cav-4-amidinobenzylamide (Figure S1), #8 in Lam van et al.[14]). After intraperitoneally (*i.p.*) treatment, mice accepted a bolus treatment of only 2.5 mg/kg of inhibitor **MI-1148**, whereas 15 mg/kg were tolerated in case of compound **MI-1851** (no higher dose was tested with the latter compound). With the exception of the P1 residue, the new inhibitor **17** is otherwise structurally identical with compound **MI-1851**. Therefore, to investigate the influence of the P1 group of this inhibitor type on toxicity, inhibitor **17** was tested under identical conditions as used previously. For this purpose, inhibitor **17** was converted into a physiologically better acceptable hydrochloride salt as described previously.[21] On the first day, the mice (n = 4, two male and two female) were *i.p.* treated with 5 mg/kg inhibitor, and always 24 hours later with 10, 15, and 20 mg/kg. Doses of 5, 10 and 15 mg/kg with inhibitor **17** were well tolerated, in case of 20 mg/kg one of the mice died. This suggests that the P1 Amia group possesses a similar influence on the toxicity profile of these substrate-analogue furin inhibitors in mice as the Amba residue.

The Mas-Related GPCR-X2 as Potential Off-Target of Benzamidine-Derived Furin Inhibitors

In our previous studies we could not find a correlation between the toxicity and inhibitory potency against furin for these peptidic benzamidine-derived furin inhibitors.[14,21] This suggested a different, but so far unknown mechanism, underlying the toxicity of these compounds. Other groups have also reported toxic effects via a sharp drop of arterial blood pressure for various benzamidine-derivatives in rats, which were developed as thrombin inhibitors.[29,30] A benzamidine-induced mast cell degranulation leading to a strong histamine release was described as reason for the drop of blood pressure and reduced tracheal airflow causing the mortality.[30] In subsequent work, one of the groups reported that benzamidines provoke a release of histamine from mast cells via an activation of G_i proteins, because the release could be blocked by treatment with pertussis toxin (PTX), an inhibitor of the G_i protein.[31] Therefore, we were interested in assessing whether the PTX-sensitive G_i-coupled Mas-related GPCR-X2 (MRGPRX2) could be a potential off-target of our benzamidine-derived furin inhibitors. Tatemoto and colleagues[32] were the first to demonstrate expression of MRGPRX2 on human mast cells. MRGPRX2 is now known to become activated by a plethora of cationic ligands such as substance P, neuropeptide Y, or compound 48/80, collectively called basic secretagogues. It is also thought that many adverse reactions to commonly used drugs such as vancomycin, rocuronium, morphine or ciprofloxazin (to name but a few) are mediated via MRGPRX2. Activation of this receptor by basic secretagogues results in fast mast cell degranulation with histamine release.[33]

We therefore addressed the ability of four peptidic furin inhibitors described in previous studies (the strongly toxic derivative **MI-1148** and the significantly less toxic inhibitor **MI-1851**, structures given in Figure S1) and in this work (inhibitors **16** and **17**) to activate mast cells via MRGPRX2 using a recently created fluorescent reporter system derived from the previously described NPY-mRFP rat basophilic leukemia (RBL) reporter cell line[34,35] after stable transfection with human MRGPRX2 receptor cDNA. Activation by the used inhibitors, as well as by compound 48/80[36] (a polymer produced by condensation of *N*-methyl-*p*-methoxyphenethylamine with formaldehyde) used as positive control, was assessed by measuring the release of red fluorescence (preformed in granules in the NPY-mRFP reporter) into the medium 45 minutes after stimulation using a fluorescent plate reader (Figure 5).

At highest concentration of 80 μM, inhibitor **MI-1148**, but not the other three tested compounds, led to a significantly

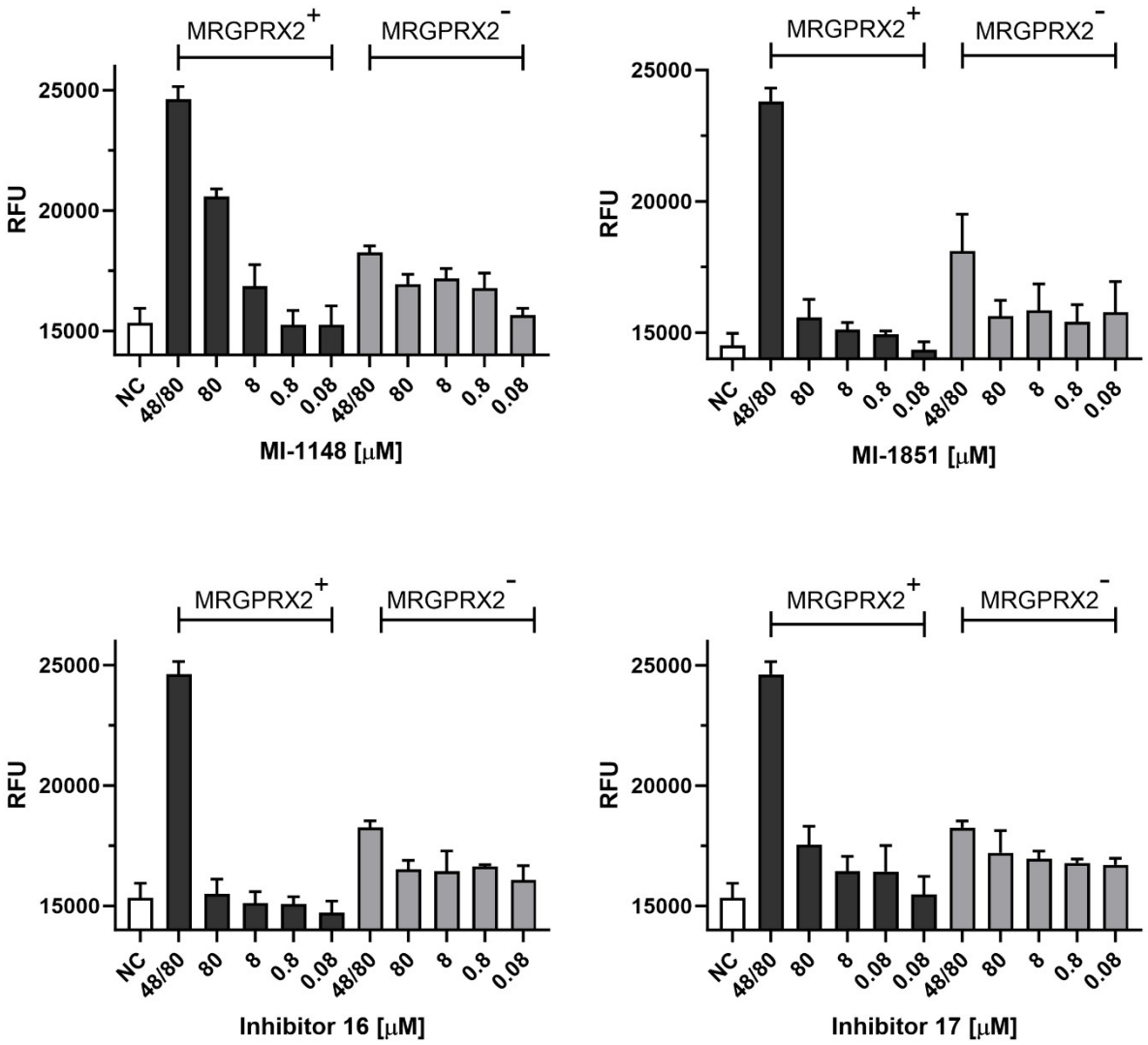

Figure 5. MRGPRX2 activation by selected furin inhibitors. MRGPRX2/NPY-mRFP stably transfected RBL cells (indicated as MRGPRX2$^+$), as well as the parental NPY-mRFP monotransfectant RBL cells (MRGPRX2$^-$) without the receptor, were incubated for 45 minutes with a tenfold serial dilution of stimulant, with concentrations ranging from 80 to 0.08 μM (corresponding to approx. 100 to 0.1 μg/mL). Supernatants were then transferred to black 96 well plates and fluorescence measured using a plate fluorimeter. Compound 48/80 was used as positive control at a concentration of 10 μg/mL, while the negative control (NC) only contained medium without stimulants. Results are mean values (+standard deviation) representative of 3 independent biological repeats, each performed in quadruplicates (N = 3, n = 4), with comparable results.

higher release of fluorescence compared with the parental non-MRGPRX2 transfected reporter cell line. This suggests a possible mechanism underlying the enhanced toxicity of the strongly multibasic inhibitor **MI-1148** containing three guanidino and one benzamidine group via activation of MRGPRX2. The relatively high concentration (80 μM) needed to elicit a measurable response is in line with the EC_{50} values needed by other, non-physiological ligands of MRGPRX2, such as ciprofloxacin (20 μM), vancomycin (40 μM) or rocuronium (500 μM).[37]

Antiviral Activity

Furin activates the precursors of the fusion proteins of many viruses including respiratory syncytial virus (RSV) F protein. RSV is the most common pathogen identified in infants and young children with acute lower respiratory infection. In some cases, typically infants aged 0–6 months, RSV can lead to bronchiolitis or pneumonia. Worldwide, it is estimated that RSV is responsible for three million hospitalizations annually, and more than 100,000 childhood deaths.[38] In addition, RSV is increasingly recognized as a pathogen that can cause serious illness in older adults and people with chronic diseases, leading to an increasing number of hospitalizations.[39] Activation of RSV F by furin is essential for virus infectivity and therefore provides a potential antiviral drug target. Therefore, we investigated the inhibitors in a virus multicycle replication assay in A549 human lung cells infected with the RSV A2 strain, as shown previously for compound **MI-1851**, which was used as reference inhibitor.[14] Cells were infected with virus and incubated in the presence of 0.5, 1 or 2.5 μM of the indicated inhibitor for 72 h. Cell supernatants were collected and virus titers determined by

plaque assay. Inhibitor **15** caused efficient inhibition of RSV titers similar to MI-1851 in a dose-dependent manner (Figure 6). The strongest antiviral efficacy was found for compound **17**, which reduced virus titers more than 2.000-fold at 1 μM and completely blocked virus replication at a concentration of 2.5 μM. Inhibitors **16** and **18** showed the lowest antiviral activity, nevertheless caused a 1.000- and 100-fold reduction in virus titer, respectively, in cells treated with 2.5 μM inhibitor (Figure 6).

In a second experiment, cells were inoculated with RSV A2 and incubated in the presence of 0.5 μM of the indicated inhibitors for 72 h. At 24, 48 and 72 h post infection cell supernatants were collected and virus titers determined by plaque assay. Again, the strongest antiviral efficacy was found for inhibitor **17**, which almost completely reduced virus replication. Inhibitor **15** reduced virus titers 100-fold at 72 h p.i. similar to MI-1851. Inhibitors **16** and **18** showed the lowest antiviral activity, nevertheless caused a 30- and 10-fold reduction in virus titer, respectively, at 72 h p.i. (Figure 7).

Furthermore, furin activates the surface glycoprotein hemagglutinin (HA) of highly pathogenic avian influenza A viruses (HPAIV) for membrane fusion. HPAIV cause serious disease in birds (fowl plague) that is highly contagious and often fatal for domestic poultry. Since 1997, there have been sporadic infections with HPAIV of subtype H5N1 in humans, usually due to direct contact with infected birds, but associated with a high

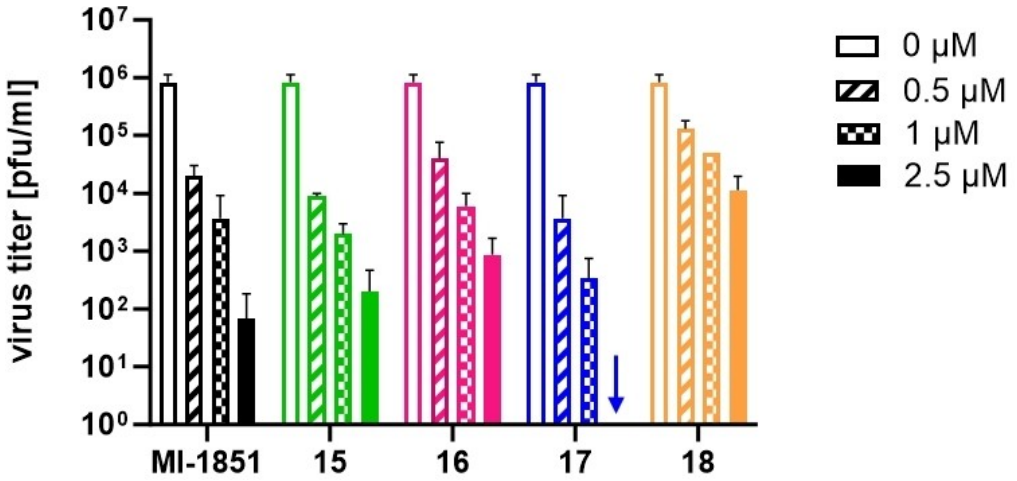

Figure 6. Antiviral potency against RSV A2 in inhibitor-treated A549 human lung cells. Cells were inoculated with virus at a MOI of 1 for 1 h, washed and incubated in absence or presence of the indicated inhibitors (0.5 μM, 1 μM or 2.5 μM) for 72 h. Cell supernatants were collected and viral titers were analyzed by plaque assay. Data are mean values + standard deviations (SD) of three independent experiments. The arrow at 2.5 μM inhibitor **17** indicates complete inhibition of virus replication.

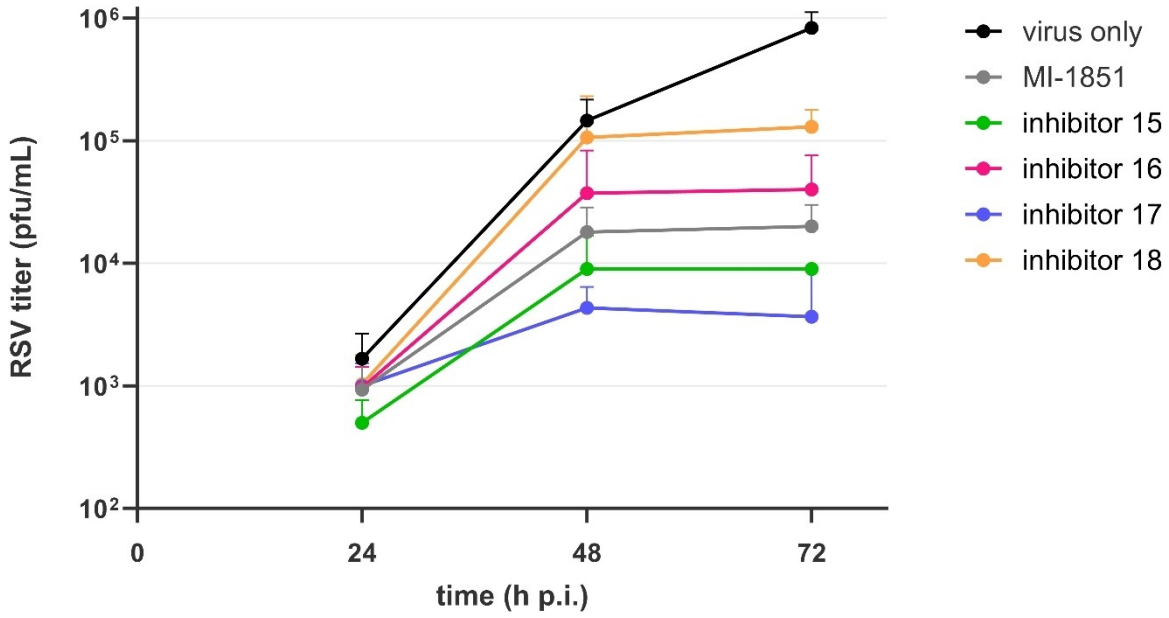

Figure 7. Inhibition of multicycle replication of RSV A2 in inhibitor-treated A549 human lung cells. Cells were inoculated with virus at a MOI of 1 for 1 h, washed and incubated in the presence of the indicated inhibitors (0.5 μM) for 72 h. At 24, 48 and 72 h post-infection (p.i.) cell supernatants were collected and viral titers were analyzed by plaque assay. Data are mean values + SD of three independent experiments (n = 3).

mortality rate of 52% (WHO/GIP, 5 January 2023). The global spread of H5 HPAIV in birds and the recurrent transmission to mammalian species including humans poses a significant human health threat with pandemic potential. As for RSV, cleavage of HA by furin is crucial for HPAIV infectivity and furin inhibition represents a potential therapeutic approach. Therefore, the antiviral activity of the inhibitors was investigated in A549 cells for the influenza A virus SC35M, which represents a HPAIV that replicates efficiently in mammalian cells. Also in this experiment, inhibitor **MI-1851** served as reference compound. A549 cells were infected with virus at a low multiplicity of infection (MOI) of 0.0001 and then incubated in the presence of inhibitors for 72 h. At indicated time points, cell supernatants were collected and virus titers were determined by plaque titration. The strongest antiviral potency was found for inhibitors **15**, **17**, and **MI-1851**, which almost completely inhibited multicycle replication of SC35M in A549 cells at a concentration of 0.5 μM (data not shown) and strongly suppressed virus growth at 0.1 μM (Figure 8A). Inhibitor **15** showed the strongest antiviral activity and reduced virus titers 10.000-fold at 48 and 72 h p.i.. The effectiveness of compound **17** was between that of compounds **15** and **MI-1851**, whereas a reduced potency was found for inhibitors **16** and **18**. To analyze cleavage of SC35M HA in inhibitor treated cells, cells were inoculated with virus at a MOI of 0.1 and incubated with different concentrations of inhibitors **15**, **17** and **MI-1851** for 24 h. Cell lysates were subjected to SDS-PAGE and Western Blot analysis using HA-specific antibodies. As shown in Figure 8B, HA0 was cleaved

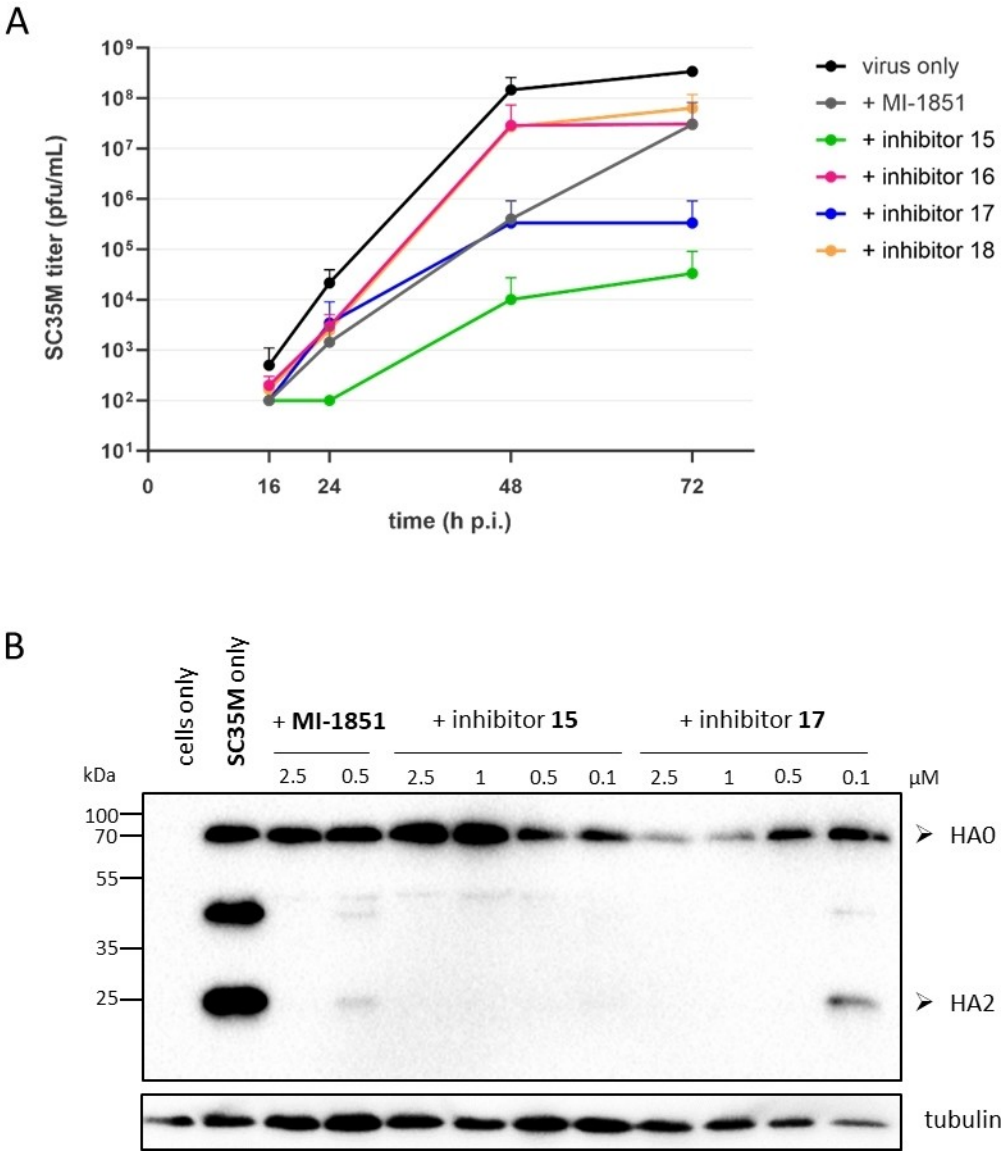

Figure 8. Inhibition of multicycle replication of influenza A strain SC35M in inhibitor-treated A549 human lung cells (A). Cells were inoculated with virus at a MOI of 0.0001 for 1 h, washed and incubated in the presence of 0.1 μM of the indicated inhibitors for 72 h. At 16, 24, 48 and 72 h post-infection (p.i.) cell supernatants were collected and viral titers were analyzed by plaque assay. Data are mean values + SD of three independent experiments. (B) Inhibition of HA0 cleavage by the reference compound **MI-1851** and inhibitors **15** and **17** at indicated concentrations relative to the control in absence of inhibitor. A549 cells were infected with SC35M at a MOI of 0.1. After a 1 h incubation, cells were treated with inhibitors and further incubated in the presence of inhibitors for 24 h. HA0 and mature cleavage products HA1 and HA2 were immunochemically detected with an H7-specific antibody in Western blot analysis.

into subunits HA1 and HA2 in untreated SC35M-infected cells. In contrast, HA0 cleavage was inhibited in inhibitor-treated cells in a dose-dependent manner.

Discussion

Crystallographic fragment screening is an important and meanwhile well-established method in the process of drug discovery. Furin is well suited for this purpose, as it usually crystallizes well in ligand-free form[16,40] applicable for soaking experiments and also in complex with a wide variety of structurally different ligands including peptidic inhibitors,[18,28] nonpeptidic small molecules[7,17,19] or even large nanobodies.[41] Since we and other groups had found toxic side effects with benzamidine-derived peptidic PC inhibitors,[21,42,43] we used this approach to identify new P1 ligands. So far, we had not succeeded in finding suitable alternative P1 residues to replace the benzamidine group, all previous variations resulted in a strong drop of inhibitory potency against furin.[21] Here, using a fragment screening approach, we could identify 1*H*-isoindol-3-amine as a strongly binding P1 group with reduced basicity, which could be converted into an aminomethyl-substituted derivative suited for incorporation in peptidic inhibitors.

The determined inhibition constants even revealed a slightly stronger inhibitory effect compared to their analogous benzamidine inhibitors. Although a slow-binding behavior was observed during the enzyme kinetic analysis under the conditions used, especially the two stronger inhibitors, **15** and **17**, bind very rapidly to furin with association rate constants $>1\cdot10^8\ M^{-1}s^{-1}$. It means that the slow-binding effect is only caused by the very low inhibitor concentrations <6 nM used in the measurements and the relatively large value for the term $1+[S]/K_m$ at a substrate concentration of 50 μM, which leads to a strong protection of the enzyme by the substrate and prohibits a rapid inhibitor binding. Based on equation 3 and despite large k_{on} values, these two conditions result in sufficiently small k_{obs} values ($\leq 0.025\ s^{-1}$) leading to the visible slow-binding phenomenon. For tightly bound inhibitors, the k_{off} values usually possess negligible small values and therefore, have only a minor influence on the k_{obs} values. Furthermore, we also tested the Amia group as potential P1 residue for trypsin-like serine proteases. For H-ᴅPhe-Pro-Amia we obtained an approximately 2.5-fold reduced inhibitory potency ($K_i=2.0\pm0.14$ nM) against thrombin compared with its benzamidine analogue H-ᴅPhe-Pro-Amba ($K_i=0.81\pm0.25$ nM). Hence, the Amia group slightly contributes to a further improved selectivity profile of these inhibitors for furin compared with thrombin. So far, we have not yet tested other proteases and therefore cannot say whether this tendency also applies to other basic PCs and trypsin-like serine proteases.

The superimposed crystal structures of furin in complex with the Amia-derived inhibitors **15** or **17** with the structure of the Amba-type inhibitor **MI-1148** (Figure 4) demonstrate that the aminomethyl substitution on the amino-isoindole fragment **F2** is well accepted. It enables an unchanged binding mode for the P5-P2 segment of these peptidic inhibitors as found in previous structures.[14,16] Furthermore, the exocyclic amidine group of the Amba inhibitor is placed almost identically as the cyclic amidine function of the Amia residue. The slightly improved furin inhibition of the Amia-derived inhibitors compared to their Amba analogues might be explained by the conformational rigidification of the Amia residue through its bicyclic structure. In addition, the Amia residue is a more space filling group through its additional CH_2-group enabling more extensive van der Waals interactions compared to Amba. A similar behavior we observed in previous studies, if valine was exchanged by *tert*-leucine at P3 position.[12]

Our original goal was to identify alternative P1 groups that lead to similar potent and less toxic furin inhibitors compared to their Amba derivatives. While the first goal has been achieved, the results in mice indicate a comparable toxicity of the new Amia derived furin inhibitor **17** and its already known Amba analogue **MI-1851**.[14] With both inhibitors, a dose of 15 mg/kg was tolerated after *i.p.* treatment. We already knew from previous studies that the strength of furin inhibition only correlates to a limited extent with the toxicity of the compounds.[14,21] Hence, we suspected that an as-yet-unknown off-target is responsible for the toxicity of these inhibitors, rather than the furin inhibition. As other groups have reported toxic effects of benzamidine-derived protease inhibitors through a G_i-dependent histamine release associated with a drop in blood pressure,[30,31] we speculated, if the MRGPRX2 could be an off-target for these furin inhibitors. Our results reveal that the toxic effects of the strongly multibasic inhibitor **MI-1148** in mice may be explained at least in part by activation of MRGPRX2. Our RBL reporter cell line contains NPY-mRFP preformed in granules, which is rapidly released upon activation of the MRGPRX2 receptor. RBL cells have been reported to barely express mRNA for the rat homologue MrgprB3. However, as reported by Lazki-Hagenbach, some studies have demonstrated cellular responses to Mrgpr-activating ligands.[44] We therefore sought to assess the effect of the furin inhibitors on the parental NPY-mRFP transfectant lacking the MRGPRX2 in parallel. As can be seen from Figure 5, activation by the reference compound 48/80 only resulted in a consistent cellular activation in the case of MRGPRX2$^+$ cells. Similar results were obtained with the highest 80 μM concentration of inhibitor **MI-1148**. This suggests that the activation seen with **MI-1148** is indeed caused by engagement of the human receptor, and not by endogenous rat receptors. The other three tested furin inhibitors did not appear to induce a significant degranulation of the NPY-mRFP reporter, with or without MRGPRX2. However, these results are only a preliminary indication that this receptor may be a relevant off-target for the particularly toxic furin inhibitor **MI-1148**.

The slightly enhanced inhibitory potency of inhibitor **17** compared to its Amba analogue **MI-1851** correlates with a somewhat stronger antiviral potency against RSV in A549 cells. Low micromolar concentrations of inhibitor **17** reduce RSV titers by several orders of magnitude (Figures 6–7). In contrast, the most potent antiviral effect against influenza virus SC35M was achieved by inhibitor **15**, although in this experiment, inhibitor **17** also proved to be slightly more effective than the Amba

inhibitor **MI-1851**. It is possible that in addition to furin other basic PCs like PC5/6 or PC7 are involved to varying degrees in the activation of the surface proteins of these viruses, resulting in slight differences in antiviral effectiveness of these inhibitors.

In summary, using a crystallographic fragment screening we identified an 1*H*-isoindol-3-amine as new anchor group for the S1 pocket of furin. Its further derivatization provided the Amia group, which could be incorporated in peptidic furin inhibitors. Their furin-bound crystal structure is nearly identical as previously observed for their Amba analogues. In enzyme kinetic studies with soluble furin, these inhibitors possess a slightly enhanced inhibitory potency compared to the known Amba derivatives, which also resulted in an improved antiviral potency against the tested furin-dependent viruses. For the first time, the MRGPRX2 was identified as potential off-target of certain benzamidine-based furin inhibitors. This supports our previously described assumption that the inhibition of furin itself is not the main cause of the toxic effect observed for certain inhibitors, making furin a potential target for the development of new antiinfectives.

Experimental Section

General Information

Amino acid derivatives, reagents and solvents were purchased from Acros Organics, Alfa Aesar, Bachem, BLDpharm, Carbolution, Fisher Scientific, Fluorochem, Iris Biotech, Merck KGaA or Roth and used without further purification.

Analytical HPLC measurements were performed on a Primaide (VWR, Hitachi) system (column: NUCLEODUR C18 ec, 5 μm, 100 Å, 4.6 mm×250 mm, Macherey-Nagel) with 0.1 % TFA in water (solvent A) and 0.1 % TFA in acetonitrile (solvent B) as eluents using a linear gradient with an increase of 1 % B/min at a flow rate of 1 mL/min and detection at 220 nm.

Purifications via preparative HPLC were performed on a Knauer Azura system (pump P 2.1 L equipped with pump head E4099AB, detector UVD 2.1 L, Knauer GmbH, Berlin, Germany) using the same solvents as described above for the analytical HPLC and a linear gradient with an increase of 0.5 % B/min at a flow rate of 20 mL/min (detection at 220 nm). After preparative HPLC, all inhibitors were obtained as lyophilized TFA-salts in a purity > 95 %.

ESI mass spectra were measured on a QTrap 2000 ESI spectrometer (Applied Biosystems), HR-ESI mass spectra were determined using a micrOTOF-Q III spectrometer (Bruker Daltonics, Billerica, MA), and HR-APCI mass spectra were acquired with a LTQ-FT Ultra mass spectrometer (Thermo Fischer Scientific). The resolution was set to 100.000.

NMR-spectra were measured on a ECA500 (^{1}H: 500 MHz, ^{13}C: 126 MHz) with the respective deuterated solvent as internal standard. The chemical shifts δ are reported in ppm and the coupling constants J are given in Hz. Resonance multiplicities are abbreviated as follows: s = singlet, br s = broad singlet, d = doublet, t = triplet, q = quartet, dd = doublet of doublet, dt = doublet of triplet, ddt = doublet of doublet of triplet, m = multiplet).

Certain reactions were performed in a Discover SP microwave in 10 mL or 35 mL reaction tubes (CEM GmbH, Kamp-Lintfort, Germany).

Synthesis of Precursors

2,4-bis(bromomethyl)benzonitrile (6)[45]

2,4-dimethylbenzonitrile **5** (515 mg, 3.93 mmol, 1.0 eq.) and NBS (1400 mg. 7.86 mmol, 2.0 eq.) were dissolved in 10 mL acetonitrile in a microwave vessel. AIBN (3 mg, 0.02 mmol, 0.005 eq.) was added and the solution heated in a microwave for 4 h at 140 °C. The solvent was removed *in vacuo*. The product was purified by preparative HPLC. Yield: 378 mg (1.3 mmol, 33 %) as colorless oil. **HPLC**: 27.3 min, start at 30 % solvent B; purity: > 94 %; **^{1}H NMR** (500 MHz, DMSO-D6) δ 7.88 (d, J = 8.0 Hz, 1H), 7.79 (d, J = 1.7 Hz, 1H), 7.60 (dd, J = 8.0, 1.8 Hz, 1H), 4.80 (s, 2H), 4.75 (s, 2H). **^{13}C NMR** (126 MHz, DMSO-D6) δ 148.4, 145.5, 132.4, 125.3, 125.2, 117.5, 107.4, 62.3, 61.0. **MS** (ESI, positive): calcd. m/z: 286.89; found m/z: 309.89 $[M+Na]^+$.

2,4-bis((1,3-dioxoisoindolin-2-yl)methyl)benzonitrile (7)

Compound **6** (1.00 g, 3.5 mmol, 1.0 eq.) and potassium phthalimide (1.41 g, 7.6 mmol, 2.2 eq.) were treated with 50 mL of DMF and the slurry was heated for 1 h to 100 °C providing a clear solution. After cooling, the solvent was removed *in vacuo* and the remaining solid was washed with water on a glass frit and dried *in vacuo* (1.29 g, 3.1 mmol white solid, 88.6 %). **HPLC**: 28.6 min, start at 30 % solvent B; purity: 96.8 %; **^{1}H NMR** (500 MHz, $CDCl_3$) δ 7.91–7.87 (m, 2H), 7.85–7.81 (m, 2H), 7.79–7.75 (m, 2H), 7.75–7.71 (m, 2H), 7.62 (d, J = 8.0 Hz, 1H), 7.47–7.41 (m, 1H), 7.38 (dd, J = 8.0, 1.6 Hz, 1H), 5.06 (s, 2H), 4.82 (s, 2H). **^{13}C NMR** (126 MHz, $CDCl_3$) δ 167.8, 167.8, 141.9, 140.2, 134.5, 134.4, 133.8, 132.0, 132.0, 128.7, 128.1, 123.8, 123.7, 117.0, 111.5, 41.2, 39.8. **MS** (ESI, positive): calcd. m/z: 421.11; found m/z: 422.14 $[M+H]^+$.

6-(aminomethyl)-1H-isoindol-3-amine·2 TFA (8)

Compound **7** (836 mg, 2.0 mmol, 1 eq) was dissolved in 30 mL of ethanol and treated with methylamine (8 M solution in EtOH, 4.96 mL, 39.7 mmol, 20 eq.). The solution was refluxed for 3 h and then cooled to room temperature. The solution was acidified with 10 % aqueous TFA, afterwards the solvents were removed *in vacuo*. The product was purified by preparative HPLC and lyophilized (264 mg, 0.68 mmol white lyophilized solid, 34 % yield). **HPLC**: 9.1 min, start at 1 % solvent B; purity: > 99 %; **^{1}H NMR** (500 MHz, DMSO-D6) δ 10.70 (br s, 1H), 9.71 (s, 1H), 9.46 (s, 1H), 8.41 (br s, 3H), 8.23 (d, J = 8.2 Hz, 1H), 7.81 (s, 1H), 7.72 (dd, J = 8.2, 1.2 Hz, 1H), 4.84 (s, 2H), 4.22 (s, 2H). **^{13}C NMR** (126 MHz, DMSO-D6) δ 163.1, 144.6, 139.7, 129.0, 128.1, 123.9, 123.8, 51.0, 42.1. **MS** (ESI, positive): calcd. m/z: 161.10; found m/z: 162.05 $[M+H]^+$. **HRMS** (ESI, positive): calcd. m/z: 161.0953; found m/z: 162.1028 $[M+H]^+$).

Benzyl Allylcarbamate (10)[46]

Allylamine (0.50 g, 8.8 mmol, 1.05 eq) was dissolved in 10 mL DMF at 0 °C and treated with Cbz-OSu (2.07 g, 8.3 mmol, 1.00 eq) followed by dropwise addition of DIPEA (1.49 mL, 8.8 mmol, 1.05 eq) within 10 min. The mixture was warmed to room temperature and stirred for another 2.5 h. The solvent was removed *in vacuo* and the residue dissolved with ethyl acetate. The organic phase was washed three times with aqueous 5 % $KHSO_4$, once with brine and dried over anhydrous $MgSO_4$. The solvent was removed *in vacuo* (1.39 g, 7.27 mmol of a light-yellow oil, 87.4 %). **HPLC**: 27.3 min, start at 20 % solvent B; purity: > 99 %; **^{1}H NMR** (500 MHz, DMSO-D6) δ 7.45–7.25 (m, 6H), 5.79 (ddt, J = 17.2, 10.3, 5.2 Hz, 1H), 5.12 (dq, J = 17.2, 1.8 Hz, 1H), 5.08–4.98 (m, 3H), 3.63 (ddt, J = 5.9, 5.3, 1.7 Hz, 2H). **^{13}C NMR** (126 MHz, DMSO-D6) δ 156.0, 137.2, 135.5,

128.3, 127.7, 127.6, 114.8, 65.2, 42.6. **MS** (ESI, positive): calcd. m/z: 191.09; found m/z: 214.09 $[M+Na]^+$.

2-(4-(3-aminopropyl)phenyl)acetic Acid (12)

2-(4-iodophenyl)acetic acid **9** (500 mg, 1.91 mmol, 1.00 eq), compound **10** (703 mg, 3.68 mmol, 1.93 eq), K_2CO_3 (330 mg, 2.39 mmol, 1.25 eq) and $Pd(OAc)_2$ (21 mg, 0.95 mmol, 0.05 eq) were dissolved in 15 mL DMF and heated to 140 °C for 30 min. After cooling to room temperature, the mixture was filtered and the solvent removed *in vacuo*, giving the crude intermediate **11** (HPLC: 22.1 min, start at 30% solvent B, MS (ESI, positive): calcd. m/z: 325.13; found m/z: 326.29 $[M+H]^+$). Intermediate **11** was dissolved in 50 mL ethanol and treated with 50 mg 10% Pd/C. The mixture was stirred under hydrogen atmosphere for 40 h. The catalyst was removed by filtration and the solvent removed *in vacuo*. The residue was dissolved in concentrated aqueous $NaHCO_3$ and extracted thrice with ether. The aqueous layer was acidified with aqueous 5% $KHSO_4$ and extracted 4 times with ethyl acetate. The combined organic layer was washed with brine and dried over anhydrous $MgSO_4$. The solvent was removed *in vacuo*. Due to incomplete removal of the Cbz group during hydrogenation, the residue was dissolved in 33% HBr in acetic acid and stirred for 2 h at room temperature. After precipitating in cold ether, the obtained solid was purified with preparative HPLC (102 mg, 0.33 mmol white lyophilized solid, 17.4% yield). **HPLC**: 20.1 min, start at 1% solvent B; purity: 99.1%; **^{1}H NMR** (500 MHz, DMSO-D6) δ 12.27 (br s, 1H), 7.73 (br s, 3H), 7.43–6.87 (m, 4H), 3.52 (s, 2H), 2.92–2.71 (m, 2H), 2.67–2.58 (m, 2H), 1.94–1.71 (m, 2H). **^{13}C NMR** (126 MHz, DMSO-D6) δ 172.6, 139.0, 132.7, 129.4, 128.1, 40.2, 38.4, 31.4, 28.7. **MS** (ESI, positive): calcd. m/z: 193.11; found m/z: 194.16 $[M+H]^+$.

2-(4-(3-((tert-butoxycarbonyl)amino)propyl)phenyl)acetic Acid (13)[47]

Compound **12** (86 mg, 280 μmol, 1.00 eq) was dissolved in a mixture of 5 mL dioxane and 5 mL 0.5 M NaOH and cooled to 0 °C. Boc_2O (67 mg, 308 μmol, 1.10 eq) was dissolved in 5 mL dioxane and added dropwise. The mixture was then warmed to room temperature and stirred overnight. The mixture was acidified with conc. aqueous citric acid and extracted thrice with ethyl acetate. The combined organic layers were washed with brine and dried over $MgSO_4$. The solvent was removed *in vacuo* (68 mg, 232 μmol light-yellow oil which crystallized at room temperature, 82.9% yield). **HPLC**: 20.6 min, start at 30% solvent B; purity: 98.1%; **^{1}H NMR** (500 MHz, $CDCl_3$) δ 7.21–7.07 (m, 4H), 4.56 (br s, 1H), 3.61 (s, 2H), 3.13 (br s, 2H), 2.74–2.49 (m, 2H), 1.89–1.70 (m, 2H), 1.44 (s, 9H). **^{13}C NMR** (126 MHz, $CDCl_3$) δ 176.7, 140.7, 131.2, 129.5, 128.8, 77.4, 40.7, 32.8, 31.7, 28.5. **MS** (ESI, positive): calcd. m/z: 293.16; found 294.38 $[M+H]^+$. **HRMS** (ESI, positive): calcd. m/z: 293.1627; found m/z: 316.1515 $[M+Na]^+$.

Synthesis of Inhibitor 17

The synthesis of the inhibitors was performed by a combination of SPPS and solution synthesis, as described for analogous Amba derivatives.[14,21] Here, only the synthesis of inhibitor **17** is briefly described. The synthesis started from the side-chain protected precursor **14** (Scheme 3) prepared by standard Fmoc-SPPS on 295 mg 2-CTC-resin (loading 1.6 mmol/g). The initial resin loading with Fmoc-Cav(Boc)-OH provided an effective loading of 0.76 mmol/g, which was used to calculate the amounts of subsequent amino acid couplings. Its synthesis was reported in detail in the supporting information of our previous publication.[14] The crude intermediate **14** was obtained by mild acidic cleavage (1% TFA in DCM) from resin, followed by neutralization with DIPEA. After removing of the solvent *in vacuo*, the crude product (approximately 0.347 mmol based on initial loading) was used without further purification. The crude intermediate and 203 mg (0.522 mmol, 1.5 eq) of compound **8** were dissolved in 3 mL DMF and treated with 298 mg (0.573 mmol, 1.65 eq) PyBOP, 265 mg (1.56 mmol, 4.5 eq) 6-Cl-HOBt and 242 μL (1.39 mmol, 4.0 eq) DIPEA at 0 °C. The mixture was allowed to warm to room temperature and stirred overnight. The Boc-protected crude intermediate was obtained by removing the solvent *in vacuo* (HPLC 20.7 min, start at 30% solvent B). The oily residue was treated with 3 mL TFA/H_2O/triisopropylsilane (95 : 2.5 : 2.5, v/v/v) and stirred for 7.5 hours until full deprotection was observed via analytical HPLC. The product was isolated by precipitation in cold diethyl ether and subsequent purification by preparative HPLC (101 mg, 0.082 mmol of white lyophilized solid, 23.6% yield), **HPLC**: 22.25 min, start at 1% solvent B; purity: >99% (Figure S2); **^{1}H NMR** (500 MHz, DMSO-d6) δ [ppm] = 11.30 (br s, 2H), 10.64 (br s, 1H), 9.64 (s, 1H), 9.44 (s, 1H), 8.70 (t, J = 6.0 Hz, 1H), 8.49 (d, J = 8.1 Hz, 1H), 8.29 (d, J = 7.3 Hz, 1H), 8.17–8.08 (m, 2H), 7.80 (br s, 8H), 7.64 (d, J = 9.1 Hz, 1H), 7.60 (s, 1H), 7.53–7.11 (m, 9H), 4.75 (s, 2H), 4.55–4.45 (m, 2H), 4.44–4.35 (m, 2H), 4.33 (d, J = 6.1 Hz, 2H), 4.24 (d, J = 9.0 Hz, 1H), 3.86–3.75 (m, 4H), 3.53–3.44 (m, 2H), 2.11–1.99 (m, 2H), 1.98–1.73 (m, 2H), 0.86 (s, 9H). **^{13}C NMR** (126 MHz, DMSO-d6) δ [ppm] = 171.3, 170.8, 170.6, 170.0, 163.4, 159.1 (q, $^2J_{C\text{-}F}$ = 31.7 Hz, CF_3COO^-), 158.5, 158.4, 157.0, 145.6, 144.6, 135.3, 135.3, 129.2, 127.2, 127.1, 126.7, 123.5, 121.9, 117.0 (q, $^1J_{C\text{-}F}$ = 298.8 Hz, CF_3COO^-), 73.2, 72.9, 59.6, 50.8, 49.9, 49.6, 43.7, 42.1, 41.5, 34.3, 29.9, 29.8, 26.4. (Figure S3), **MS** (ESI, positive): calcd. m/z: 779.43; found m/z: 780.47 $[M+H]^+$. **HRMS** (APCI, positive): calcd. m/z: 779.4303; found m/z: 780.4374 $[M+H]^+$.

The other inhibitors **15**, **16**, and **18** were prepared by the same strategy from appropriate precursors, their analytical data are provided in the supporting information (Table S1, Figure S2).

Kinetic Measurements

Measurements with soluble human furin[48] were performed in 96-well black FluoroNunc MaxiSorp plates plates (Nunc, Langenselbold, Germany) at room temperature for 30 min using a Tecan Spark microplate reader (Tecan Deutschland GmbH, Crailsheim, Germany). Each well contained 20 μL of the substrate Ac–Arg–Arg–Tle–Arg–Arg–AMC[26] (dissolved and diluted in water) and 160 μL buffer (100 mM HEPES, 0.2% Triton X-100, 2 mM $CaCl_2$, 0.02% NaN_3, and 1 mg/mL BSA, pH 7.0), and 2 μL inhibitor dissolved in DMSO. The measurements were started by the addition of 20 μL furin solution (total assay volume 202 μL, final furin concentration 95 pM).

For all inhibitors nonlinear progress curves have been observed, which were fitted to eq 2 for slow-binding inhibition providing the v_s values used for K_i calculations (v_0: constant initial velocity in absence of inhibitor; k_{obs}: apparent first-order rate constant; d: displacement of the fluorescence signal from zero at t = 0). The K_i values were calculated by fitting the steady state velocity v_s as function of the inhibitor concentrations using eq 1. The required V_{max} and K_m values were obtained from Michaelis-Menten plots determined on the same plate. Eq 3 was used to calculate the association rate constant k_{on} from plots of the determined k_{obs} values as function of the inhibitor concentration. The dissociation rate constant k_{off} was calculated according to eq 4 using the values for K_i and k_{on} determined before.

$$v_s = V_{max} \cdot [S]/[K_m \cdot (1 + [I]/K_i) + [S]] \quad \text{(eq 1)}$$

$$[P] = v_S\, t + (v_0 - v_S)\, [1 - \exp(-k_{obs}\, t)]/k_{obs} + d \quad \text{(eq 2)}$$

$$k_{obs} = k_{on}\ [I]/(1 + [S]/K_m) + k_{off} \quad \text{(eq 3)}$$

$$K_i = k_{off}/k_{on} \quad \text{(eq 4)}$$

X-ray Crystallography

Expression of homogenously glycosylated furin in stably transfected HEK293S-cells and the purification from conditioned medium was performed as described previously.[15,16,28] For crystallization, equal volumes (~10 mg/mL in 10 mM HEPES, pH 7.5, 100 mM NaCl, 2 mM $CaCl_2$) and crystallization solution (100 mM MES, 200 mM K/NaH_2PO_4, pH 5.5-6.0 and 2 M NaCl) were mixed and equilibrated against the reservoir (3.0-3.2 M NaCl) in vapor diffusion experiments at 18–20 °C as described in previous studies.[16]

The optimized soaking solution for crystallographic fragment screening and soaking of substrate-like inhibitors was either 1.0 M NaCl, 200 mM MES/NaOH pH 5.5, 1 mM $CaCl_2$, 10% (w/v) PEG8000 and 20% (v/v) DMSO or 3.13 M NaCl, 100 mM MES/NaOH, pH 5.5, 200 mM NaH_2PO_4, 1 mM $CaCl_2$, 20% (v/v) DMSO and were supplemented with the specific inhibitors.[15,19] Fragments were soaked overnight at concentrations as indicated in Figure S5. If the crystals appeared optically damaged, soaking was repeated at 20 mM fragment concentration. The inhibitors **15** and **17** were soaked 1 h at concentrations of 5 mM and 2 mM, respectively. Crystals were flash cooled in liquid N_2.

Diffraction data collection of fragment-soaked crystals was performed at the synchrotron beam line BL14.2 (BESSY-II) of the Helmholtz-Zentrum Berlin (HZB).[49,50] The typical data collection strategy comprised 1800 images in 0.1° increments with exposure time of 0.1 s. For **F1** and **F2** additional datasets were collected with 0.2 s exposure time that were used for model building later (see below). The data were automatically processed using XDS[51] with XDSAPP (v2.0)[52] and programs of the CCP4 program suite (v.7.0.078).[53] For automated refinement[23] the structure of unliganded furin (PDB-ID 5JXG[16]) was used as starting model including the calcium and sodium ions. Hit identification was performed in two rounds. First, the datasets were analyzed with PanDDA[24] for initial hit identification. 93 datasets of equally treated ligand-free furin crystals were included in the analysis to compute the ground state model. In the second round, datasets with binding events were excluded to compute the ground state model. All automated refinement and hit finding procedures were also carried out at the Helmholtz-Zentrum Berlin.

Diffraction data of inhibitors **15** and **17** soaked crystals were collected at the synchrotron beam lines ID23-1[54] and ID30B[55] of the European Synchrotron Radiation Facility (ESRF). The data were processed using XDS[51] with XDSAPP (v2.0)[52] and programs of the CCP4 program suite (v.7.0.078).[53] Data collection statistics of the structures of furin bound to **F1** and **F2** as well as to inhibitors **15** and **17** are shown in Table S2. COOT (v.0.8.9.2)[56] was used for model building. Refinement was performed in PHENIX (v1.20.1)[57] using the PDB-ID 5JXG[16] for fragments **F1** and **F2** and the PDB-ID 5JXH[16] for inhibitor-bound structures as initial models. R_{free}-reflections (initially generated up to 1.0 Å) were transferred to the data sets prior refinement start. Geometry restraints of the inhibitors were obtained from the PRODRG-server[58] and from the GRADE webserver.[59] Electron density omit maps were calculated in PHENIX (v1.20.1) after one round of torsion angle simulated annealing refinement with omitted ligands. PyMOL was used for molecular graphics (http://www.pymol.org) and structural alignments. Structure factors and coordinates of the complexes of furin with fragments **F1**, **F2** and inhibitors **15** and **17** have been deposited as PDB entries 8B4V, 8B4W, 8B4X, and 8OYH, respectively.

Toxicity Studies in Mice

The toxicity study with inhibitor **17** was conducted by Pharmacology Discovery Services Taiwan, Ltd. as previously described,[14,21] the conditions are given in the supporting information. All animal experiments performed in the manuscript were conducted in compliance with institutional guidelines.

Assessment of MRGPRX2 Activation

RBL-2H3 cells stably transfected with NPY-mRFP[34] alone or with NPY-mRFP/MRGPRX2 double transfectants were cultured in complete EMEM medium,[35] supplemented with the selection antibiotics G418 (1 mg/mL. InvivoGen) or G418 (1 mg/mL) and Blasticidin S (30 μg/mL, Gibco ThermoScientific Fisher), respectively. The day before the assay, cells were harvested with trypsin/EDTA (Merck) from a 70–80% confluent flask, resuspended at a density of $2x10^6$ cells/mL in complete medium omitting the selection antibiotics, and 50 μL of this suspension, seeded into each well of a cell culture-grade 96-well flat-bottomed plate. 50 μL containing the stimuli to be tested, containing 180 μM, 18 μM, 1,8 μM and 0,18 μM of inhibitor were added to the 50 μL of medium containing the adherent cells. After 45 minutes, 70 μL of supernatant were carefully transferred to a black microplate (96F nontreated black plates, NUNC/ThermoScientific Fisher) avoiding bubbles, and fluorescence measured (λex/em 542/585 nm) using a CLARIOstar plus microplate reader (BMG Labtech, Ortenberg, Germany). Compound 48/80 (Merck/Sigma-Aldrich) was used at a final concentration of 10 μg/mL as positive control.[36]

Determination of Antiviral Activities

RSV infections and inhibition of multicycle replication: The antiviral potency against RSV in infected A549 cells was determined as described in our previous publications.[14,60]

Influenza A SC35M infections and inhibition of multicycle replication: SC35M infection experiments were carried out in Dulbecco's Modified Eagle Medium (DMEM, Gibco, Thermo Fisher Scientific, Paisley, UK) supplemented with 0.1% Bovine Serum Albumin (BSA, Bovine Serum Albumin solution 30% in saline, IgG free, SIGMA-ALDRICH Co.), penicillin, streptomycin (Pen Strep, Gibco, Thermo Fisher Scientific, Paisley, UK) and 2 mM L-Glutamine (L-Glutamine 200 mM, Gibco, Thermo Fisher Scientific, Paisley, UK). Recombinant influenza A virus SC35M/H7N7 (reverse genetics system kindly provided by Jürgen Stech (Friedrich Loeffler Institute, Greifswald – Isle of Riems, Germany). SC35M was propagated in MDCK-II cells in infection medium (DMEM (Gibco) supplemented with 0.1% bovine serum albumin (BSA), glutamine, and antibiotics). Cell supernatants were cleared from cell debris by low-speed centrifugation and stored as virus stocks at −80 °C. For inhibition of SC35M multicycle replication, adenocarcinomic human alveolar basal epithelial cells A549 were grown in DMEM supplemented with 10% fetal bovine serum (FBS, Gibco, Thermo Fisher Scientific, Paisley, UK), penicillin, streptomycin and 2 mM L-Glutamine until 95% confluence. Growth medium was removed, cells were washed with PBS def. and infected with SC35M at a MOI of 0.0001 for 1 h at 37 °C, 5% CO_2. Inoculum was removed, cells were washed with PBS def. and fresh medium with or without inhibitors was added. Cells were then further incubated at 37 °C, 5% CO_2 for 72 h in total. 50 μL cell supernatant was collected at different time points and stored at −20 °C until plaque assay titration.

Plaque assay titration SC35M: Madin-Darby canine kidney cells II (MDCKII) were cultured until 95% cell confluence was reached, growth medium was aspirated and cells washed with PBS. Cells were then inoculated with 10-fold serial dilutions of cell supernatants in Dulbecco's Modified Eagle Medium (Gibco) supplemented with 0.1% Bovine Serum Albumin (BSA), penicillin, streptomycin and 2 mM L-Glutamine and incubated at 37 °C, 5% CO_2 for 1 hour. Inoculum was removed and replaced with 50% v/v double-concentrated MEM (2xMEM (Gibco) supplemented with 0.6% BSA solution 30% in saline, IgG free, SIGMA-ALDRICH Co.), penicillin, streptomycin (Pen Strep, Gibco, Thermo Fisher Scientific, Paisley, UK), 4 mM L-Glutamine (L-Glutamine 200 mM, Gibco, Thermo Fisher Scientific, Paisley, UK) and 50% cellulose solution (Avicel (Sigma Aldrich) 2.5% w/v in double-distilled H_2O) and incubated for 48 hours at 37 °C, 5% CO_2. Overlay was removed and cells were washed three times with PBS. Cells were then fixated with 4% w/v *p*-formaldehyde in PBS at 4 °C for 30 minutes. Next, cells were permeabilized with 0.3% Triton-X-100 (SIGMA-ALDRICH) and stained with Giemsa's Azur eosin methylene blue solution (Merck Millipore). Virus infected areas were counted and plaque forming units per mL calculated.

$$\text{PFU per mL} = \frac{\text{number of plaques} \times \text{reciprocal dilution factor}}{\text{volume inoculum in mL}}$$

SDS-PAGE and Western blot: A549 cells were infected with SC35M at a MOI of 0.1 in DMEM supplemented with 0.1% BSA, penicillin, streptomycin and 2 mM L-Glutamine for 1 h at 37 °C, 5% CO_2. Inoculum was removed, cells were washed with PBS def. and then treated with inhibitors at the indicated concentrations and incubated in the presence of inhibitors for 24 h at 37 °C, 5% CO_2. Subsequently, cells were washed with PBS, lysed in Cell Lysis buffer (CellLytic M, Sigma-Aldrich Pty Ltd, Merck KGaA) supplemented with 0.1% v/v Protease Inhibitor-Cocktail (Protease Inhibitor-Cocktail derived from bovine lung, Sigma-Aldrich Pty Ltd, Merck KGaA) mixed with 6x reducing Laemmli buffer and heated at 95 °C for 10 min. Cell lysates were subjected to SDS-PAGE (12% gel), transferred to a polyvinylidene difluoride (PVDF) membrane (GE Healthcare, Freiburg, Germany), and detected with primary antibodies (polyclonal rabbit serum against H7, Sino Biological Inc., Monoclonal Anti-α-Tubulin antibody produced in mouse SIGMA-ALDRICH Co.) and species-specific peroxidase-conjugated secondary antibodies (DAKO). Proteins were visualized using the ChemiDoc XRS+ system with Image Lab software (Bio-Rad).

Supporting Information

Additional references cited within the Supporting Information.[61]

Abbreviations

AIBN	azobisisobutyronitrile
Amba	4-amidinobenzylamide
Amia	6-(aminomethyl)-1*H*-isoindole-3-amine
APCI	atmospheric pressure chemical ionization
Cav	canavanine
Cbz	benzyloxycarbonyl
DCM	dichloromethane
DIPEA	N,N-diisopropylethylamine
DMF	N,N-dimethylformamide
ESI	electrospray ionization
6-Cl-HOBt	1-Hydroxy-6-chloro-benzotriazole
i.p.	intraperitoneal
MOI	multiplicity of infection
NBS	*N*-bromosuccinimide
PC	proprotein convertase
PyBOP	(Benzotriazol-1-yloxy)tripyrrolidinophosphonium hexafluorophosphate
RSV	respiratory syncytial virus
SPPS	solid-phase peptide synthesis
TFA	trifluoroacetic acid
TIS	triisopropylsilane
Tle	*tert*.leucine

Acknowledgements

We thank Iris Lindberg (University of Maryland, Baltimore) for providing the furin used in enzyme kinetic measurements. The authors acknowledge the provision of synchrotron beamtime at the ESRF (ID23-1 and ID30B) and at the Helmholtz-Zentrum Berlin (HZB, BL14.2) and thank the scientific staff for assistance. We also thank the Helmholtz-Zentrum Berlin for the travel support. T. S., E. B.-F., G. K., and F.H.F. obtained funding from the LOEWE Center DRUID (Novel Drug Targets against Poverty-Related and Neglected Tropical Infectious Diseases). G. K. was additionally funded by the BMBF project Frag4Lead FKZ 05K16RM1. S.O.D. obtained funding by the Austrian Science Fund (FWF): M 2730 and P36648-B, which is gratefully acknowledged. Open Access funding enabled and organized by Projekt DEAL.

Conflict of Interest

The authors declare no conflict of interest.

Keywords: fragment screening · furin inhibitors · proprotein convertases · crystal structure analysis · proteolytic activation of viruses

[1] G. Thomas, *Nat. Rev. Mol. Cell Biol.* **2002**, *3*, 753–766.
[2] N. G. Seidah, A. Prat, *Nat. Rev. Drug Discovery* **2012**, *11*, 367–383.
[3] P. Stawowy, H. Meyborg, D. Stibenz, N. Borges Pereira Stawowy, M. Roser, U. Thanabalasingam, J. P. Veinot, M. Chretien, N. G. Seidah, E. Fleck, K. Graf, *Circulation* **2005**, *111*, 2820–2827.
[4] F. Couture, F. D'Anjou, R. Day, *Biomol. Concepts* **2011**, *2*, 421–438.
[5] Z. He, A. M. Khatib, J. W. M. Creemers, *Oncogene* **2022**, *41*, 1252–1262.
[6] Y. Zhang, X. Gao, X. Bai, S. Yao, Y. Z. Chang, G. Gao, *Transl. Neurodegener.* **2022**, *11*, 39.
[7] L. E. J. Douglas, J. A. Reihill, M. W. Y. Ho, J. M. Axten, N. Campobasso, J. L. Schneck, A. R. Rendina, K. M. Wilcoxen, S. L. Martin, *Cell Chem. Biol.* **2022**, *29*, 947–957.
[8] E. E. A. Osman, A. Rehemtulla, N. Neamati, *J. Med. Chem.* **2022**, *65*, 2747–2784.
[9] W. Garten in *Activation of Viruses by Host Proteases* (Eds.: E. Böttcher-Friebertshäuser, W. Garten, H. D. Klenk), Springer International Publishing, Cham, **2018**.

[10] D. Bestle, M. R. Heindl, H. Limburg, T. van Lam, O. Pilgram, H. Moulton, D. A. Stein, K. Hardes, M. Eickmann, O. Dolnik, C. Rohde, H. D. Klenk, W. Garten, T. Steinmetzer, E. Böttcher-Friebertshäuser, *Life Sci. Alliance* **2020**, *3*, e202000786.
[11] R. Essalmani, J. Jain, D. Susan-Resiga, U. Andréo, A. Evagelidis, R. M. Derbali, D. N. Huynh, F. Dallaire, M. Laporte, A. Delpal, P. Sutto-Ortiz, B. Coutard, C. Mapa, K. Wilcoxen, E. Decroly, T. Nq Pham, A. Cohen, N. G. Seidah, *J. Virol.* **2022**, e0012822.
[12] K. Hardes, G. L. Becker, Y. Lu, S. O. Dahms, S. Köhler, W. Beyer, K. Sandvig, H. Yamamoto, I. Lindberg, L. Walz, V. von Messling, M. E. Than, W. Garten, T. Steinmetzer, *ChemMedChem* **2015**, *10*, 1218–1231.
[13] G. L. Becker, Y. Lu, K. Hardes, B. Strehlow, C. Levesque, I. Lindberg, K. Sandvig, U. Bakowsky, R. Day, W. Garten, T. Steinmetzer, *J. Biol. Chem.* **2012**, *287*, 21992–22003.
[14] T. V. van Lam, M. R. Heindl, C. Schlutt, E. Böttcher-Friebertshäuser, R. Bartenschlager, G. Klebe, H. Brandstetter, S. O. Dahms, T. Steinmetzer, *ACS Med. Chem. Lett.* **2021**, *12*, 426–432.
[15] S. O. Dahms, T. Haider, G. Klebe, T. Steinmetzer, H. Brandstetter, *ACS Chem. Biol.* **2021**, *16*, 1692–1700.
[16] S. O. Dahms, M. Arciniega, T. Steinmetzer, R. Huber, M. E. Than, *Proc. Natl. Acad. Sci. USA* **2016**, *113*, 11196–11201.
[17] S. O. Dahms, G. S. Jiao, M. E. Than, *ACS Chem. Biol.* **2017**, *12*, 1211–1216.
[18] S. O. Dahms, K. Hardes, T. Steinmetzer, M. E. Than, *Biochemistry* **2018**, *57*, 925–934.
[19] S. O. Dahms, G. Schnapp, M. Winter, F. H. Büttner, M. Schlepütz, C. Gnamm, A. Pautsch, H. Brandstetter, *ACS Chem. Biol.* **2022**, *17*, 816–821.
[20] J. Schiebel, N. Radeva, S. G. Krimmer, X. Wang, M. Stieler, F. R. Ehrmann, K. Fu, A. Metz, F. U. Huschmann, M. S. Weiss, U. Mueller, A. Heine, G. Klebe, *ACS Chem. Biol.* **2016**, *11*, 1693–1701.
[21] T. Ivanova, K. Hardes, S. Kallis, S. O. Dahms, M. E. Than, S. Künzel, E. Böttcher-Friebertshäuser, I. Lindberg, G. S. Jiao, R. Bartenschlager, T. Steinmetzer, *ChemMedChem* **2017**, *12*, 1953–1968.
[22] G. L. Becker, F. Sielaff, M. E. Than, I. Lindberg, S. Routhier, R. Day, Y. Lu, W. Garten, T. Steinmetzer, *J. Med. Chem.* **2010**, *53*, 1067–1075.
[23] J. Schiebel, S. G. Krimmer, K. Röwer, A. Knörlein, X. Wang, A. Y. Park, M. Stieler, F. R. Ehrmann, K. Fu, N. Radeva, M. Krug, F. U. Huschmann, S. Glöckner, M. S. Weiss, U. Mueller, G. Klebe, A. Heine, *Structure* **2016**, *24*, 1398–1409.
[24] N. M. Pearce, T. Krojer, A. R. Bradley, P. Collins, R. P. Nowak, R. Talon, B. D. Marsden, S. Kelm, J. Shi, C. M. Deane, F. von Delft, *Nat. Commun.* **2017**, *8*, 15123.
[25] J. Lessel, *Pharmazie* **1993**, *48*, 812–816.
[26] T. V. van Lam, T. Ivanova, I. Lindberg, E. Böttcher-Friebertshäuser, T. Steinmetzer, K. Hardes, *Anal. Biochem.* **2022**, *655*, 114836.
[27] A. Boyar, R. E. Marsh, *J. Am. Chem. Soc.* **1982**, *104*, 1995–1998.
[28] S. O. Dahms, K. Hardes, G. L. Becker, T. Steinmetzer, H. Brandstetter, M. E. Than, *ACS Chem. Biol.* **2014**, *9*, 1113–1118.
[29] B. Kaiser, J. Hauptmann, F. Markwardt, *Pharmazie* **1987**, *42*, 119–121.
[30] L. Peternel, M. Stempelj, M. Cerne, A. Zega, A. Obreza, M. Oblak, G. Drevensek, M. V. Budihna, L. Stanovnik, U. Urleb, *Thromb. Haemostasis* **2006**, *95*, 294–300.
[31] M. Stempelj, M. Zorko, L. Peternel, U. Urleb, I. Ferjan, *Eur. J. Pharmacol.* **2006**, *538*, 182–187.
[32] K. Tatemoto, Y. Nozaki, R. Tsuda, S. Konno, K. Tomura, M. Furuno, H. Ogasawara, K. Edamura, H. Takagi, H. Iwamura, M. Noguchi, T. Naito, *Biochem. Biophys. Res. Commun.* **2006**, *349*, 1322–1328.
[33] H. Ogasawara, M. Noguchi, *Cells* **2021**, *10*, 2906.
[34] F. H. Falcone, D. Wan, N. Barwary, R. Sagi-Eisenberg, *Immunol. Rev.* **2018**, *282*, 47–57.
[35] N. J. S. Barwary, D. Wan, F. H. Falcone, *Methods Mol. Biol.* **2020**, *2163*, 163–170.
[36] S. W. Kashem, H. Subramanian, S. J. Collington, P. Magotti, J. D. Lambris, H. Ali, *Eur. J. Pharmacol.* **2011**, *668*, 299–304.
[37] B. D. McNeil, *Front. Immunol.* **2021**, *12*, 676354.
[38] Y. Li, X. Wang, D. M. Blau, M. T. Caballero, D. R. Feikin, C. J. Gill, S. A. Madhi, S. B. Omer, E. A. F. Simões, H. Campbell, A. B. Pariente, D. Bardach, Q. Bassat, J.-S. Casalegno, G. Chakhunashvili, N. Crawford, D. Danilenko, L. A. H. Do, M. Echavarria, A. Gentile, A. Gordon, T. Heikkinen, Q. S. Huang, S. Jullien, A. Krishnan, E. L. Lopez, J. Markić, A. Mira-Iglesias, H. C. Moore, J. Moyes, L. Mwananyanda, D. J. Nokes, F. Noordeen, E. Obodai, N. Palani, C. Romero, V. Salimi, A. Satav, E. Seo, Z. Shchomak, R. Singleton, K. Stolyarov, S. K. Stoszek, A. von Gottberg, D. Wurzel, L.-M. Yoshida, C. F. Yung, H. J. Zar, H. Nair, *Lancet* **2022**, *399*, 2047–2064.
[39] R. Nuwer, *Nature* **2023**, *621*, S58-S59.
[40] K. H. Pearce, L. K. Overton, R. T. Gampe, G. B. Barrett, J. D. Taylor, D. D. McKee, N. Campobasso, R. T. Nolte, R. A. Reid, *Acta Crystallogr. Sect. F* **2019**, *75*, 239–245.
[41] S. O. Dahms, J. W. Creemers, Y. Schaub, G. P. Bourenkov, T. Zogg, H. Brandstetter, M. E. Than, *Sci. Rep.* **2016**, *6*, 34303.
[42] H. Gagnon, S. Beauchemin, A. Kwiatkowska, F. Couture, F. D'Anjou, C. Levesque, F. Dufour, A. R. Desbiens, R. Vaillancourt, S. Bernard, R. Desjardins, F. Malouin, Y. L. Dory, R. Day, *J. Med. Chem.* **2014**, *57*, 29–41.
[43] A. Kwiatkowska, F. Couture, C. Levesque, K. Ly, S. Beauchemin, R. Desjardins, W. Neugebauer, Y. L. Dory, R. Day, *ChemMedChem* **2016**, *11*, 289–301.
[44] P. Lazki-Hagenbach, H. Ali, R. Sagi-Eisenberg, *Cells* **2021**, *10*.
[45] M. M. Hammoud, M. Khattab, M. Abdel-Motaal, J. van der Eycken, R. Alnajjar, H. S. Abulkhair, A. A. Al-Karmalawy, *J. Biomol. Struct. Dyn.* **2023**, *41*, 5199–5216.
[46] A. A. Schleppnik, C. D. Gutsche, *J. Org. Chem.* **1960**, *25*, 1378–1386.
[47] R. Baker, W. R. Carling, P. D. Leeson, J. D. Smith (MERCK SHARP & DOHME [GB]), EP0386839 (A2), **1990**.
[48] M. M. Kacprzak, J. R. Peinado, M. E. Than, J. Appel, S. Henrich, G. Lipkind, R. A. Houghten, W. Bode, I. Lindberg, *J. Biol. Chem.* **2004**, *279*, 36788–36794.
[49] U. Mueller, N. Darowski, M. R. Fuchs, R. Forster, M. Hellmig, K. S. Paithankar, S. Puhringer, M. Steffien, G. Zocher, M. S. Weiss, *J. Synchrotron Radiat.* **2012**, *19*, 442–449.
[50] J. Wollenhaupt, T. Barthel, G. M. A. Lima, A. Metz, D. Wallacher, E. Jagudin, F. U. Huschmann, T. Hauß, C. G. Feiler, M. Gerlach, M. Hellmig, R. Förster, M. Steffien, A. Heine, G. Klebe, U. Mueller, M. S. Weiss, *J. Visualized Exp.* **2021**, e62208.
[51] W. Kabsch, *Acta Crystallogr. Sect. D* **2010**, *66*, 125–132.
[52] M. Krug, M. S. Weiss, U. Heinemann, U. Mueller, *J. Appl. Crystallogr.* **2012**, *45*, 568–572.
[53] M. D. Winn, C. C. Ballard, K. D. Cowtan, E. J. Dodson, P. Emsley, P. R. Evans, R. M. Keegan, E. B. Krissinel, A. G. Leslie, A. McCoy, S. J. McNicholas, G. N. Murshudov, N. S. Pannu, E. A. Potterton, H. R. Powell, R. J. Read, A. Vagin, K. S. Wilson, *Acta Crystallogr. Sect. D* **2011**, *67*, 235–242.
[54] C. Mueller-Dieckmann, M. W. Bowler, P. Carpentier, D. Flot, A. A. McCarthy, M. H. Nanao, D. Nurizzo, P. Pernot, A. Popov, A. Round, A. Royant, D. de Sanctis, D. von Stetten, G. A. Leonard, *Eur. Phys. J. Plus* **2015**, *130*, 70.
[55] A. A. McCarthy, R. Barrett, A. Beteva, H. Caserotto, F. Dobias, F. Felisaz, T. Giraud, M. Guijarro, R. Janocha, A. Khadrouche, M. Lentini, G. A. Leonard, M. Lopez Marrero, S. Malbet-Monaco, S. McSweeney, D. Nurizzo, G. Papp, C. Rossi, J. Sinoir, C. Sorez, J. Surr, O. Svensson, U. Zander, F. Cipriani, P. Theveneau, C. Mueller-Dieckmann, *J. Synchrotron Radiat.* **2018**, *25*, 1249–1260.
[56] P. Emsley, B. Lohkamp, W. G. Scott, K. Cowtan, *Acta Crystallogr. Sect. D* **2010**, *66*, 486–501.
[57] P. D. Adams, P. V. Afonine, G. Bunkoczi, V. B. Chen, I. W. Davis, N. Echols, J. J. Headd, L. W. Hung, G. J. Kapral, R. W. Grosse-Kunstleve, A. J. McCoy, N. W. Moriarty, R. Oeffner, R. J. Read, D. C. Richardson, J. S. Richardson, T. C. Terwilliger, P. H. Zwart, *Acta Crystallogr. Sect. D* **2010**, *66*, 213–221.
[58] A. W. Schuttelkopf, D. M. van Aalten, *Acta Crystallogr. Sect. D* **2004**, *60*, 1355–1363.
[59] Smart, O. S., Womack, T. O., Sharff, A., Flensburg, C., Keller, P., Paciorek, W., Vonrhein, C. and Bricogne, G. **2011**, Grade, version 1.2.13, 2011, Cambridge, United Kingdom, Global Phasing Ltd., https://www.globalphasing.com.
[60] T. van Lam, T. Ivanova, K. Hardes, M. R. Heindl, R. E. Morty, E. Böttcher-Friebertshäuser, I. Lindberg, M. E. Than, S. O. Dahms, T. Steinmetzer, *ChemMedChem* **2019**, *14*, 673–685.
[61] F. U. Huschmann, J. Linnik, K. Sparta, M. Ühlein, X. Wang, A. Metz, J. Schiebel, A. Heine, G. Klebe, M. S. Weiss, U. Mueller, *Acta Crystallogr. Sect. F* **2016**, *72*, 346–355.

Revised manuscript received: February 21, 2024
Accepted manuscript online: February 22, 2024
Version of record online: March 11, 2024